Journal of Sound and Vibration (1999) **226**(3), 493–517
Article No. jsvi.1999.2260, available online at http://www.idealibrary.com on IDEAL®

NON-LINEAR DYNAMICS OF A TWO-DIMENSIONAL AIRFOIL BY INCREMENTAL HARMONIC BALANCE METHOD

A. RAGHOTHAMA AND S. NARAYANAN

Machine Dynamics Laboratory, Department of Applied Mechanics, Indian Institute of Technology, Madras Chennai, 600036, *India*

(*Received* 13 *August* 1998, *and in final form* 18 *March* 1999)

Periodic oscillations and bifurcations of a two-dimensional airfoil in plunge and pitching motions with cubic pitching stiffness in incompressible flow is investigated using the incremental harmonic balance (IHB) method. The bifurcations are obtained with the parametric continuation technique and the stability of the periodic motions is investigated using the Floquet theory. The autonomous non-linear system of the airfoil undergoes initial Hopf bifurcation leading to limit cycle oscillation as the airspeed parameter is increased. Further increase in the airspeed causes symmetry breaking, saddle-node and period-doubling bifurcations leading to chaos. The frequency of the limit cycle oscillation is also determined in the IHB method.

1. INTRODUCTION

A number of investigations have been carried out in recent years for the aeroelastic analysis of airfoils and missile control surfaces with structural and free play non-linearities. Such non-linearities have significant effects on the aeroelastic response which exhibits diverse motions like periodic response, including harmonic and subharmonic motions, chaotic motion, divergent flutter and damped stable motions. Dowell [1] has shown that a buckled plate with fluid flow over its upper surface can exhibit chaotic motion. Many issues such as interaction between a number of modes, sensitivity of the time step used in numerical simulation, effect of initial and sufficient conditions for onset of chaos have been discussed. The effects of structural non-linearities on the response of bluff body oscillators and airfoils in transonic flow have been discussed in Dowell and Ilgamov [2]. Yang and Zhao [3] have performed theoretical and experimental studies to investigate the self-excited oscillations of a two-dimensional airfoil model with non-linear pitching stiffness. Free play non-linearity was considered in their study and the single-term harmonic balance method was used to ascertain the stable and unstable limit cycle motions. Digital simulation was used for flutter analysis and comparison between the theoretical and experimental results were made. Zhao and Yang [4] have investigated the chaotic behavior of two-dimensional airfoils with cubic pitching

0022-460X/99/380493 + 25 $30.00/0

stiffness in incompressible flow. They have shown that such a system exhibited chaotic behavior through a series of period-doubling bifurcations in certain parameter ranges. The boundaries of different motion types are shown in the parameter map of airspeed and elastic axis position by numerical simulation. Tang and Dowell [5] have studied the flutter instability and forced response of a non-rotating helicopter blade model with NACA-0012 airfoil and a pitch-free play structural non-linearity. The effects of various initial disturbance amplitudes on the forced response behavior were discussed. The results showed that the system exhibited both limit cycle oscillation and chaotic behavior. A two-dimensional airfoil with either a bilinear or cubic structural non-linearity in pitch and subjected to incompressible flow has been analyzed by evaluating the aerodynamic forces on the airfoil using Wagner's function by Price *et al.* [6]. The equations were solved by numerical integration using a finite-difference method and in a semi-analytical manner by using a dual-input describing function. For the system with cubic non-linearity it was shown that chaos could exist which was confirmed by computing the Lyapunov exponents. The chaotic motion was obtained for both bilinear and cubic non-linearities. Kim and Lee [7] have also analyzed the dynamics of a two-dimensional airfoil with freeplay non-linearity and have observed limit cycle and chaotic motions which were highly influenced by the pitch-plunge frequency ratio. An experimental model which closely approximated the three-degrees-of-freedom typical airfoil section in two-dimensional, incompressible flow was constructed to validate the theoretical results by Conner *et al.* [8]. The theoretical response was determined by time marching of the governing equations using a standard Runge–Kutta algorithm in conjunction with Henon's method. The effect of free play on the system response was examined numerically and experimentally.

In this paper, the periodic motions of self-excited two-dimensional airfoil with cubic pitching stiffness are investigated by the incremental harmonic balance (IHB) method. The IHB method was developed by Cheung and Lau [9] to obtain periodic solutions of non-linear structural vibration problems based on an incremental Hamilton's principle. The method was applied to the problem of non-linear beam vibration with different boundary conditions and superharmonics, subharmonics and internal resonances were obtained. Lau *et al.* [10] have applied a variable parameter incrementation method to determine the parametric instability boundaries of beams and columns with geometric non-linearities. The boundaries of the qualitatively different solution regions of the Duffing's oscillator in the parametric space were constructed by the IHB method by Leung and Fung [11]. Chen *et al.* [12] have used the IHB method to get the limit cycle motions of a self-excited Van der Pol oscillator. Lau and Yuen [13] have used the IHB method to obtain the response diagrams of Van der Pol oscillators and coupled Van der Pol oscillators. The IHB method was modified by Leung and Chui [14] by reversing the order of the incrementation and linearization to obtain the periodic motions of a system of coupled Duffing oscillators linked through a linear spring. They also used an improved arc-length parametric continuation technique to trace the bifurcations and obtain the response diagrams.

The model for the dynamics of the airfoil adopted in this paper is essentially the same as that of Zhao and Yang [4]. The cubic pitching stiffness is used so as to

correspond to the panel flutter model under inplane loads [1]. This can also approximate to a large extent free play non-linearities. As in the paper of Zhao and Yang [4] the unsteady aerodynamics forces involving the inertial and velocity terms are neglected for simplicity. While Zhao and Yang [4] have obtained the different types of responses essentially by numerical integration, this paper is devoted to a systematical tracing of the bifurcation diagrams and identification of the types of bifurcations by a stability analysis using the Floquet theory. For this purpose the IHB method is used to obtain the periodic solutions of various orders and path following procedure to trace the response diagrams. The improved arc-length parametric continuation technique of Leung and Chui [14] is adopted for the path following. The periodic and subharmonic motions obtained by the IHB method compare very well with those obtained by numerical integration. The airfoil undergoes an initial Hopf bifurcation giving rise to limit cycle motion which further undergoes symmetry breaking, saddle-node and period-doubling bifurcations leading to chaotic motion. Chaotic motion is investigated in terms of phase planes, Poincare' sections and Lyapunov exponents by numerical integration.

2. NON-LINEAR MODEL OF A TWO-DIMENSIONAL AIRFOIL

Non-linear aeroelastic problems provide a rich source of static and dynamic instabilities and associated limit cycle motions. In aircraft design practice, structural non-linearities and concentrated non-linear elements such as in all moving tails, control surfaces and external stores are important to be included in the dynamic analysis. A two-dimensional airfoil in incompressible flow with non-linear stiffness and linear viscous damping is shown in Figure 1. The equations of motion of the airfoil with two-degrees-of-freedom in pitch and plunge are given by [15]

$$m\ddot{h} + S\ddot{\alpha} + K_h h = Q_1, \tag{1}$$

$$S\ddot{h} + I\ddot{\alpha} + K_\alpha \alpha = Q_2, \tag{2}$$

where h is the plunging displacement, α is the pitch angle, the over dots indicate the order of differentiation with respect to time t, m is the mass per unit span, S is the static moment, I is the mass moment of inertia about the elastic axis of the airfoil, and K_h is the stiffness coefficient in plunge and K_α is pitching stiffness coefficient. The unsteady aerodynamic force Q_1 and moment Q_2 can be expressed in terms of the Theodorsen functions as [3]

$$\begin{aligned} Q_1 &= -\pi\rho b^2(V\dot{\alpha} + \ddot{h} - ab\ddot{\alpha}) - 2\pi\rho VbC(k)[V\alpha + \dot{h} + (0{\cdot}5 - a)b\dot{\alpha}], \\ Q_2 &= \pi\rho b^2[ab(V\dot{\alpha} + \ddot{h} - ab\ddot{\alpha}) - 0{\cdot}5Vb\dot{\alpha} - b^2\ddot{\alpha}/8] \\ &\quad + 2\pi\rho Vb^2(0{\cdot}5 + a)C(k)[V\alpha + \dot{h} + (0{\cdot}5 - \alpha)b\dot{\alpha}]. \end{aligned} \tag{3}$$

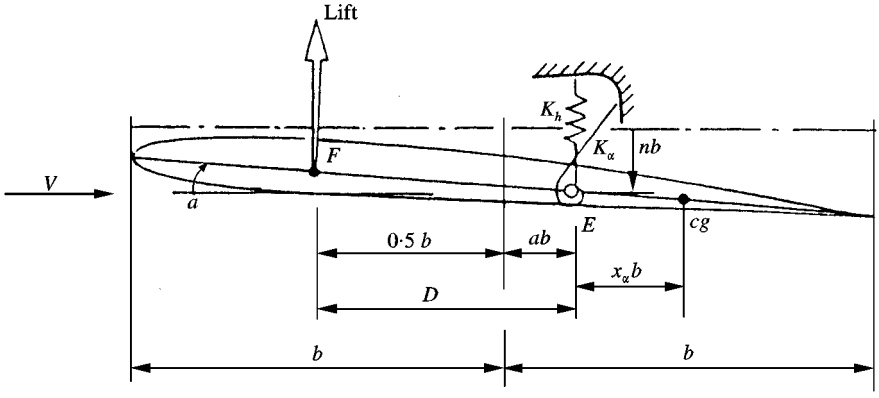

Figure 1. Two-dimensional airfoil.

In the above equations ρ is the air density, V is the air speed, b is the half-chord length of the airfoil, ab is the stream-wise distance of the pitch axis from the mid-chord point (Figure 1), $C(k)$ is the Theodorsen function, $k = \omega b/V$ is the reduced frequency and ω is the frequency. Introducing non-dimensional time $\tau = \omega_\alpha t$ and neglecting the unsteady aerodynamic terms on the right-hand side of equations (1) and (2) containing the acceleration and velocity terms as considered by Zhao and Yang [4], the equations of motion can be transformed as

$$\mu(\mathrm{d}^2 x_1/\mathrm{d}\tau^2) + \mu x_\alpha(\mathrm{d}^2 x_2/\mathrm{d}\tau^2) + \mu(\omega_h/\omega_\alpha)^2 x_1 = -2\, v\alpha, \tag{4}$$

$$\mu x_\alpha(\mathrm{d}^2 x_1/\mathrm{d}\tau^2) + \mu r_\alpha^2(\mathrm{d}^2 x_2/\mathrm{d}\tau^2) + \mu r_\alpha^2 x_2 = (1 + 2a)\, v\alpha, \tag{5}$$

where $x_1 = h/b$ is the plunging displacement divided by b, $x_2 = \alpha$ is the pitching angle, $v = V/b\omega_\alpha$ is the non-dimensional airspeed parameter, $\mu = m/(\pi\rho b^2)$ is the non-dimensional mass parameter, ab as already defined is the distance of elastic axis E from the mid-chord length, $(0{\cdot}5 + a)\ b$ is the distance of E from the aerodynamic center F, $x_\alpha b$ is the distance of the center of gravity from E, $r_\alpha b$ is the radius of gyration of the airfoil with respect to E, and $\omega_h = k_h/m$ and $\omega_\alpha = k_\alpha/I_\alpha$ are the eigenfrequencies of the constrained one-degree-of-freedom systems associated with the linear plunging and pitching motions respectively. By taking the numerical values of the parameters to be $\mu = 20$, $a = -0{\cdot}1$, $b = 1$ m, $x_\alpha = 0{\cdot}25$, $r_\alpha^2 = 0{\cdot}50$, $(\omega_h/\omega_\alpha)^2 = 0{\cdot}2$, $\omega_h = 28{\cdot}10$ Hz and $\omega_\alpha = 62{\cdot}80$ Hz and introducing a viscous damping term and a cubic pitching stiffness in equations (1) and (2), and approximating equation (3) by neglecting the inertial and velocity terms, equations (4) and (5) can be reduced to the following form:

$$\ddot{x}_1 + 0{\cdot}25\,\ddot{x}_2 + 0{\cdot}10\,\dot{x}_1 + 0{\cdot}20\,x_1 + 0{\cdot}10\,vx_2 = 0, \tag{6}$$

$$0{\cdot}25\,\ddot{x}_1 + 0{\cdot}50\,\ddot{x}_2 + 0{\cdot}10\,\dot{x}_2 + 0{\cdot}50\,x_2 + ex_2^3 - \mathrm{d}vx_2 = 0. \tag{7}$$

The over dots now represent the order of differentiation with respect to non-dimensional time τ. The above equations represent a set of autonomous equations. The periodic solutions of the above equations are obtained by the IHB method including their fundamental frequency and their stability is investigated. Chaotic motions are obtained by numerical integration. The values of the various parameters are assumed as in Zhao and Yang [4].

3. INCREMENTAL HARMONIC BALANCE METHOD

The general multi-degree-of-freedom non-linear autonomous system can be represented by the system of simultaneous non-linear differential equations of the form

$$\phi_i = \Omega^2 \ddot{x}_i + \mathrm{f}_i(x_1, x_2, \ldots, x_n, \dot{x}_1, \dot{x}_2, \ldots, \dot{x}_n, \Omega, \lambda) = 0, \quad i = 1, 2, \ldots, N, \tag{8}$$

where Ω is the frequency of oscillation of possible limit cycle motion of the autonomous system as yet undetermined. ϕ_i is a set of non-linear functions and λ is a system parameter. In the IHB method a starting solution of equation (8) is assumed as x_{i0} $(i = 1, 2, \ldots, N)$, Ω_0, λ_0 and the next solution is obtained by incrementing the initial solution as

$$x_{i1} = x_{i0} + \Delta x_{i0}, \quad i = 1, \ldots, N, \qquad \Omega_1 = \Omega_0 + \Delta\Omega_0 \quad \text{and} \quad \lambda_1 = \lambda_0 + \Delta\lambda_0. \tag{9}$$

Expanding equation (8) in Taylor series about the initial state the linearized equations in terms of the increments can be written in matrix form as

$$B\,\Delta\ddot{X} + C\,\Delta\dot{X} + K\,\Delta X = R - (2\Omega_0\,\ddot{X}_0 + Q)\,\Delta\Omega - P\,\Delta\lambda, \tag{10}$$

where **B** is a diagonal matrix with diagonal elements Ω_0^2, $X_0 = \{x_{10}, x_{20}, \ldots, x_{N0}\}^{\mathrm{T}}$, $\Delta X = \{\Delta x_{10}, \Delta x_{20}, \ldots, \Delta x_{N0}\}^{\mathrm{T}}$,

C and **K** are the Jacobian matrices corresponding to $\dot{x}_i$ and x_i respectively. **Q** and **P** are the vectors containing the derivative of f_i with respect to Ω and λ respectively, and **R** is a residue vector containing the higher order terms and the superscript T indicates transpose. Since x_{i0} is the assumed initial periodic solution, it can be approximated by the truncated Fourier series of the form

$$x_{i0} = a_{i0} + \sum_{j=1}^{M} (a_{ij}\cos j\tau + b_{ij}\sin j\tau), \quad i = 1, 2, \ldots, N. \tag{11}$$

Likewise the increment Δx_{i0} can also be expanded in the form

$$\Delta x_{i0} = \Delta a_{i0} + \sum_{j=1}^{M} (\Delta a_{ij}\cos j\tau + \Delta b_{ij}\sin j\tau), \quad i = 1, 2, \ldots, N. \tag{12}$$

Equations (11) and (12) can be written as

$$x_{i0} = \mathbf{T}\{a_{i0}, a_{i1}, \ldots, a_{iM}, b_{i1}, \ldots, b_{iM}\}^{\mathrm{T}}, \tag{13}$$

$$\Delta x_{i0} = \mathbf{T}\{\Delta a_{i0}, \Delta a_{i1}, \ldots, \Delta a_{iM}, \Delta b_{i1}, \ldots, \Delta b_{iM}\}^{\mathrm{T}}, \tag{14}$$

where

$$\mathbf{T} = \{\cos\tau, \ldots, \cos M\tau, \sin\tau, \ldots, \sin M\tau\}. \tag{15}$$

Denoting

$$A_0 = [\{a_{10}, a_{11}, \ldots, a_{1M}, b_{11}, \ldots, b_{1M}\}^{\mathrm{T}}, \ldots, \{a_{N0}, a_{N1}, \ldots, a_{NM}, b_{N1}, \ldots, b_{NM}\}^{\mathrm{T}}]^{\mathrm{T}} \tag{16}$$

and ΔA_0 likewise in terms of Δa_{ij} and Δb_{ij}'s and substituting equations (13) and (14) in equation (10), applying the Galerkin procedure, and orthogonalizing the equations with respect to $\cos\tau, \cos 2\tau, \ldots$, etc., we get

$$\Delta A_{\mathrm{T}} \left\{ \int_0^{2\pi} X^{\mathrm{T}} [\Omega_0^2 \ddot{X} + C\dot{X} + KX] \, \mathrm{d}\tau \right\} \Delta A = \Delta A^{\mathrm{T}} \left\{ \int_0^{2\pi} X^{\mathrm{T}} R \, \mathrm{d}\tau - \int_0^{2\pi} X^{\mathrm{T}} [Q + 2\Omega_0 \ddot{X} A_0] \, \mathrm{d}\tau \, \Delta\Omega + \int_0^{2\pi} Z^{\mathrm{T}} P \, \mathrm{d}\tau \, \Delta\lambda \right\}, \tag{17}$$

where X is a $N[N(2M+1)]$ matrix with the first $2M+1$ columns of the first row, $2M+2$ to $4M+2$ columns of the second row and so on and $(N-1)(2M+1)+1$ to $N(2M+1)$ of the Nth row being the elements of vector $\mathbf{T}$ and the other elements being zero. The above equation can be written as

$$\mathbf{k}\,\Delta A = \mathbf{r} + q\,\Delta\Omega + \mathbf{p}\,\Delta\lambda, \tag{18}$$

where $\mathbf{k}$ is the Jacobian matrix, $\mathbf{r}$ is the residue vector, $\mathbf{p}$ is the parametric gradient vector and $\mathbf{q}$ is the frequency gradient vector. These matrices and vectors depend on the type of non-linearities considered for study. In the present paper cubic stiffness non-linearity in pitching is considered. The contribution to the terms in equation (18) from the linear parts of the governing equation is easy to obtain and the contribution from the non-linearity is given below:

$$r_{i0} = 2B_0, \quad r_{ia} = B_k^c, \quad r_{ib} = B_k^s, \tag{19}$$

$$[k]_{cubic} = \begin{bmatrix} k_0 & k_c & k_s \\ k_c & k_{ij}^{cc} & k_{ij}^{cs} \\ k_s & k_{ij}^{sc} & k_{ij}^{ss} \end{bmatrix}, \tag{20}$$

$$k_0 = 4A_0, \qquad k_c = 2A_j^c, \qquad k_s = 2A_j^s,$$

$$k_{ij}^{cc} = \begin{cases} 2A_0 + A_{i+j}^c & \text{if } i = j, \\ A_{i+j}^c + A_{|i-j|}^c & \text{if } i \neq j, \end{cases} \quad k_{ij}^{cs} = A_{i+j}^s - sgn(j-i)\, A_{|i-j|}^s,$$

$$k_{ij}^{sc} = A_{i+j}^s - sgn(i-j)\, A_{|j-i|}^s, \quad k_{ij}^{ss} = \begin{cases} 2A_0 - A_{i+j}^c & \text{if } i = j, \\ -A_{i+j}^c + A_{|i-j|}^c & \text{if } i \neq j. \end{cases}$$

In these expressions, B_0, B_k^c and B_k^s represent the constant coefficient, cosine coefficient and sine coefficients of the triple product x_2^3 of the assumed solution respectively. Similarly, A_0, A_k^c and A_k^s represent the constant coefficient, cosine coefficient and sine coefficient of the square product x_2^2 of the assumed solution. The expressions for these coefficients are given in Appendix A. This method is equivalent to a multi-harmonic balance procedure and a Newton–Raphson technique. Also in this equation the number of incremental unknowns is one more than the number of equations due to the additional unknown $\Delta\Omega$. However, this is solved by fixing one of the Fourier coefficients to be zero in the solution procedure. Equations (18) represent a set of linear equations in the increments ΔA and $\Delta\Omega$ at each step which can be solved iteratively.

4. STABILITY ANALYSIS

The stability of the periodic solutions obtained by the IHB method is investigated by perturbing the state variables about the steady state solutions. By perturbing the obtained steady state solution x_i by Δx_i, we get the incremental equation of the following form:

$$(\partial\phi_i/\partial\dot{x}_i)\Delta\ddot{x}_i + (\cdot\phi_i/\cdot x_i)\Delta\dot{x}_i + (\partial\phi_i/\partial x_i)\Delta x = 0, \quad i = 1, 2, \ldots, N. \tag{21}$$

These equations are linear in Δx_i's but with periodically varying coefficients in general. We can rewrite the above equation in the matrix form as

$$\dot{\eta} = D(\tau)\eta, \tag{22}$$

where $\eta = \{\Delta\dot{x}, \Delta x\}^{\mathrm{T}}$ with $\Delta x = \{\Delta x_1, \Delta x_2, \ldots, \Delta x_N\}^{\mathrm{T}}$ and $\mathbf{D}$ is a $2N \times 2N$ matrix whose elements are given by $D_{ij} = (-\partial\phi_i/\partial\dot{x}_j)/(\partial\phi_i/\partial\ddot{x}_j)$ for $i = 1, 2, \ldots, N$, $j = 1, 2, \ldots, N$, $D_{ij} = (-\partial\phi_i/\partial x_j)/(\partial\phi_i/\partial\ddot{x}_j)$ for $i = 1, 2, \ldots, N$, $j = N+1, \ldots, 2N$, $D_{ij} = \delta_{ij}$, for $i = N+1, 2N$, $j = 1, 2, \ldots, N$, and $D_{ij} = 0$ for $i = N+1, \ldots, 2N$, $j = N+1, \ldots, 2N$, and δ_{ij} is the Kronecker delta. The stability of the periodic solution can be checked by evaluating the eigenvalues of the monodromy matrix, which transforms the state vector η_n at $\tau = nT$ to η_{n+1} at $\tau = (n+1)T$, where T is the period of the periodic solution. The eigenvalues of the monodromy matrix are the Floquet multipliers corresponding to the periodic solution. The periodic

solution would be stable if all the eigenvalues of the monodromy matrix lie within the unit circle. As a system parameter is varied, the eigenvalues also move and if any one of the eigenvalues crosses the unit circle the corresponding periodic solution loses stability leading to another type of solution. The way in which the eigenvalues cross the unit circle indicates the nature of bifurcation. The monodromy matrix is obtained in this paper by a procedure outlined by Friedmann *et al.* [16] using a scheme of matrix exponentiation.

5. PATH FOLLOWING AND PARAMETRIC CONTINUATION

In order to study the bifurcations as a system parameter is varied, a path following procedure using the arc-length continuation method given by Leung and Chui [14] has been adopted. Introducing the path parameter γ, the augmenting equation can be written as

$$g(x) - \gamma = 0, \tag{23}$$

where

$$x = [\{\bar{d}\}^{\mathrm{T}}, v]^{\mathrm{T}}, \ \bar{d} = \{\{d_1^{\mathrm{T}}, d_2^{\mathrm{T}}, \ldots, d_N^{\mathrm{T}}\}^{\mathrm{T}}\} \quad \text{and} \quad d_i = \{a_{io}, a_{i1}, \ldots, a_{iN}, b_{i1}, \ldots, b_{in}\}^{\mathrm{T}}.$$

A good choice of the function $g(\mathbf{x})$ is $g(\mathbf{x}) = \mathrm{x}^{\mathrm{T}} x$. Considering the increments in $\bar{d}$, v and γ in equation (23), we get the incremental equation as

$$\sum_{j=1}^{N(2M+1)} \frac{\partial g}{\partial \bar{d}_j} \{\Delta \bar{d}_j\} + \frac{\partial g}{\partial v} \Delta v - \Delta\eta + g(\mathbf{x}) - \gamma = 0, \tag{24}$$

where $\bar{d}_j$ is the jth element of $\bar{d}$.

Considering the portion of the equilibrium path of the solution branch shown in Figure 2, the augmenting equation (23) is written as

$$g(\mathbf{x}) - \gamma = [x']^{\mathrm{T}}\{x - x_c\} = 0. \tag{25}$$

The first prediction of the new point x_u of the solution along the equilibrium path is given in terms of the two previous points x_c and x_{cc} as follows:

$$x_u = x_c + \Delta\gamma\, x', \tag{26}$$

where $x' = \{x_c - x_{cc}\}/\| x_c - x_{cc} \|$ and $\Delta\gamma$ is an arbitrary step length taken in the computation by experience.

As the system considered is autonomous, the frequency of oscillation will not be known initially. This results in one extra unknown term while adopting the Newton–Raphson method of solution in the IHB method. This is solved by fixing one of the Fourier coefficients. In this paper, the last sine coefficient of the pitching

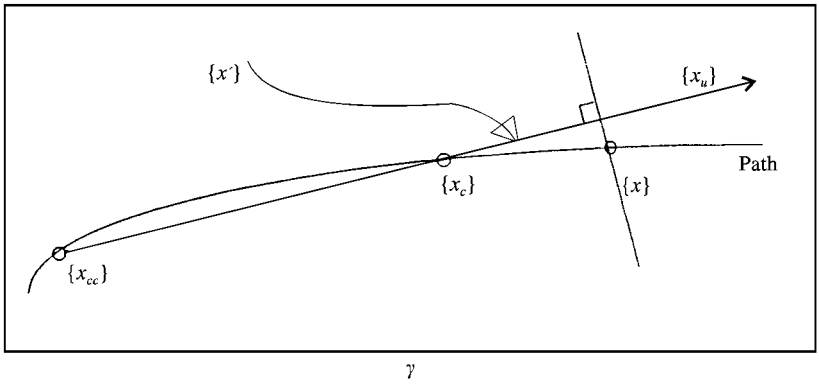

Figure 2. A portion of the equilibrium path.

mode is fixed as zero. The number of harmonics considered for obtaining periodic and subharmonic motions is discussed in the next section. Thus by fixing one of the harmonics to be zero and in that place introducing the frequency as unknown and by taking $\gamma = 0$ in equation (22) and combining these equations together, the resulting augmented incremental equation used for tracing the bifurcation diagram is given below:

$$\begin{bmatrix} -[k] & \begin{Bmatrix} q \\ p \end{Bmatrix} \\ \{\partial g/\partial \bar{d}_j\}^{\mathrm{T}} & \partial g/\partial v \end{bmatrix} \begin{Bmatrix} \Delta \bar{d} \\ \Delta \Omega \\ \Delta v \end{Bmatrix} = - \begin{Bmatrix} r \\ g - \Delta \eta \end{Bmatrix}. \tag{27}$$

6. RESULTS AND DISCUSSION

The periodic motions of the airfoil with cubic pitching stiffness described by equations (6) and (7) are obtained by the IHB method. The non-dimensional speed v is taken as the bifurcation parameter and the various bifurcations are obtained by the parametric continuation technique. The values of e and d are taken to be $e = 20$ and $d = 0{\cdot}07$. v is varied in the range from 0·05 to 16·0. This corresponds to considering a vertical section at $d = 0{\cdot}07$ in the sketch of boundaries for different types of motion in the (v, d) parameter plane given in Zhao and Yang [4]. The response diagrams corresponding to the pitch-mode oscillations are given in Figures 3(a), (b) and 4(a), (b). In Figures 3(a) and 4(a) the maximum amplitudes $x_{1\max}$ and $x_{2\max}$ plotted, while in Figures 3(b) and 4(b) the average amplitudes $(x_{1\max} + x_{1\min})/2$ and $(x_{2\max} + x_{2\min})/2$ are plotted against v. For a low value of the flow speed parameter $v = 0{\cdot}05$ shown as point "a" in the figures, the airfoil is at rest. As v is increased, it remains at rest for up to a value of $v = 3{\cdot}08$. This is marked as point "b" in the diagrams. At point "b" a Hopf bifurcation takes place as evidenced by a pair of complex conjugate eigenvalues of the monodromy matrix leaving the unit circle radially. Typical values of the complex conjugate eigenvalues in the range $v = 3{\cdot}03$ to 3·1 are given in Table 1.

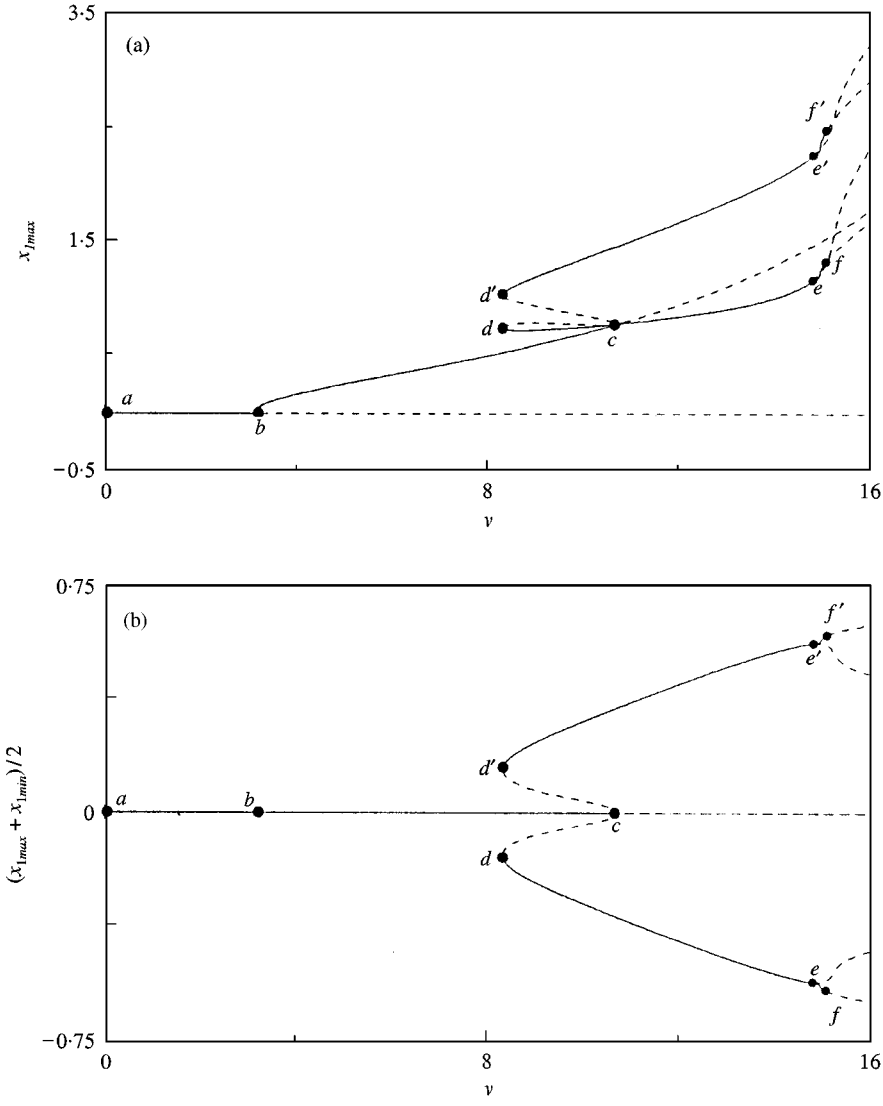

Figure 3. Response diagram in the plunge mode ($e = 20, d = 0{\cdot}07$). (a) Maximum amplitude versus v; (b) Average amplitude versus v.

The limit cycle periodic motion resulting out of the Hopf bifurcation is determined by the IHB method along with its fundamental frequency. In the first iteration, the unknown frequency is assumed to be $\Omega = 0{\cdot}42169$. The IHB procedure is started and the results of 10 iterations in terms of the error norms are shown in Table 2 at the end of which the periodic solution and its fundamental frequency are obtained with the desired accuracy. The values in Table 2 give the norm of the residue vector and the norm of the increments of the Fourier coefficients including the increment in the unknown frequency during each iteration. It is observed from the table that both of these norms are reduced substantially within a few iterations. In Table 3, the value of the unknown frequency obtained during each iteration is

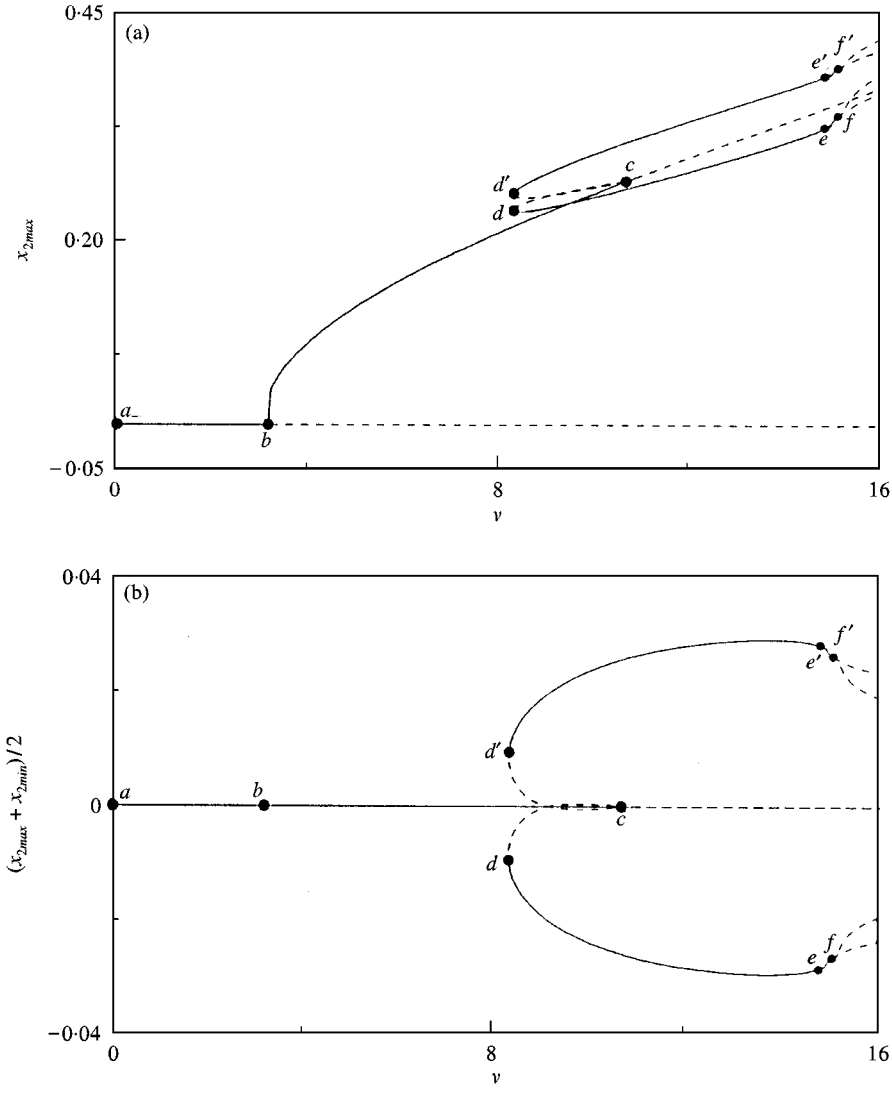

Figure 4. Response diagram in the pitch mode ($e = 20, d = 0{\cdot}07$). (a) Maximum amplitude versus v, (b) Average amplitude versus v.

given and it is seen that convergence to the fundamental frequency of the periodic solution is achieved within eight iterations. Starting with an initial guess of $\Omega = 0{\cdot}42169$, the frequency converges to a value of $\Omega = 0{\cdot}58122$ at the end of the 10th iteration.

The phase planes of the plunge and pitch-mode responses during each iteration of the IHB method are given in Figures. 5(a)–(j) and 6(a)–(j). The dotted lines in these phase planes are the solutions obtained by the IHB method during each iteration and the solid lines give phase planes obtained by numerical integration. The phase plane obtained by numerical integration is the same in all the figures but looks different because of the scale adopted for the displacement and velocity axes.

TABLE 1

Complex conjugate eigenvalues in the region $v = 3{\cdot}0$–$3{\cdot}2$

Flow speed v	Complex conjugate eigenvalues	Magnitude
3·03	− 0·490305E + 00 ± i0·737013E + 00	0·885205E + 00
3·04	− 0·507604E + 00 ± i0·752211E + 00	0·907460E + 00
3·05	− 0·524841E + 00 ± i0·767954E + 00	0·930168E + 00
3·06	− 0·542005E + 00 ± i0·784234E + 00	0·953306E + 00
3·07	− 0·559086E + 00 ± i0·801043E + 00	0·976856E + 00
3·08	− 0·576076E + 00 ± i0·818373E + 00	0·100080E + 01
3·09	− 0·592965E + 00 ± i0·836217E + 00	0·102512E + 01
3·10	− 0·609748E + 00 ± i0·854570E + 00	0·104980E + 01

TABLE 2

Typical values of the norm of residue vector and Fourier coefficients

Iteration	Norm of residue vector	Norm of increment vector
1	2·0835E-02	1·0440
2	8·1821E-02	8·1369E-01
3	1·6150E-01	3·6887E-01
4	1·4484E-02	2·7987E-01
5	9·8072E-03	7·4840E-02
6	1·8719E-03	8·7492E-02
7	9·2510E-04	4·5515E-02
8	2·9725E-04	1·2907E-02
9	2·3277E-05	6·5289E-04
10	6·6417E-08	3·501E-06

TABLE 3

Typical values of the unknown frequency at the end of each iteration with starting value of $\Omega = 4{\cdot}2169$E-001

Iteration	Frequency
1	1·3981E-001
2	5·6771E-001
3	5·8885E-001
4	5·6698E-001
5	5·6305E-001
6	5·7233E-001
7	5·7937E-001
8	5·8111E-001
9	5·8122E-001
10	5·8122E-001

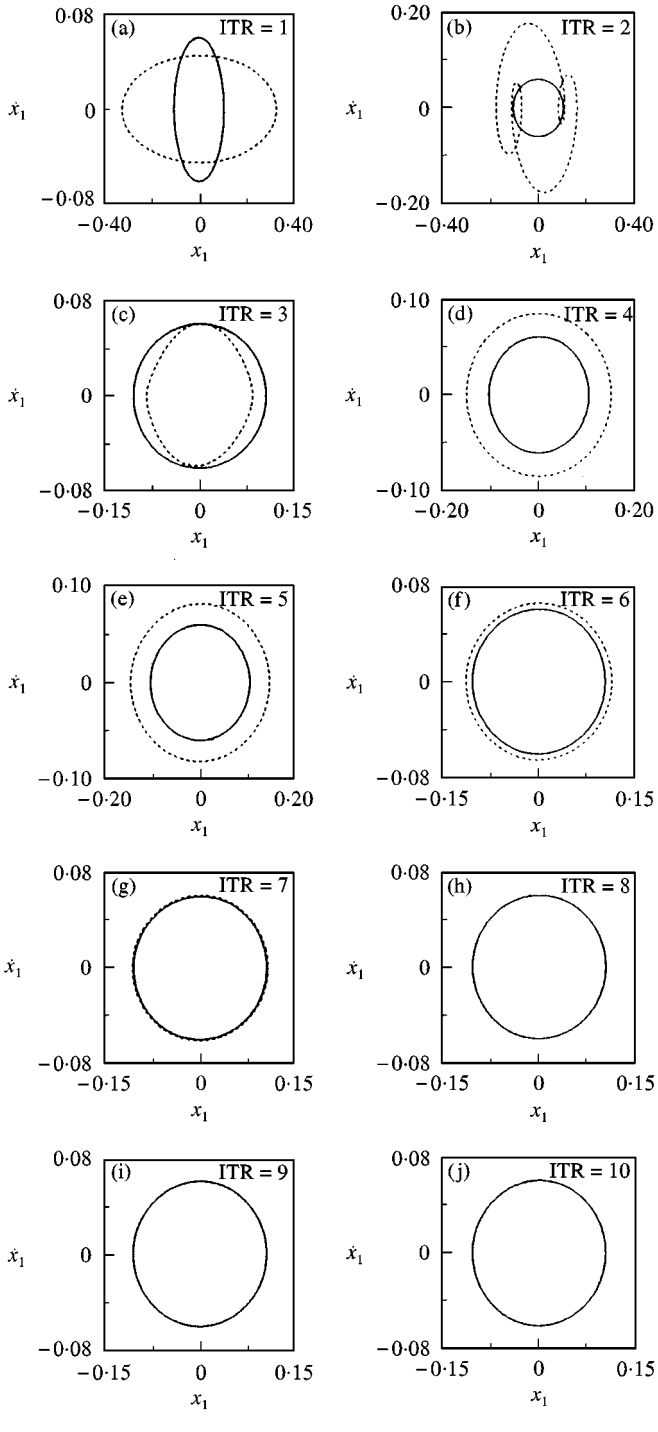

Figure 5. Convergence to limit cycle motion (plunge mode) in the IHB method $v = 3{\cdot}5$.

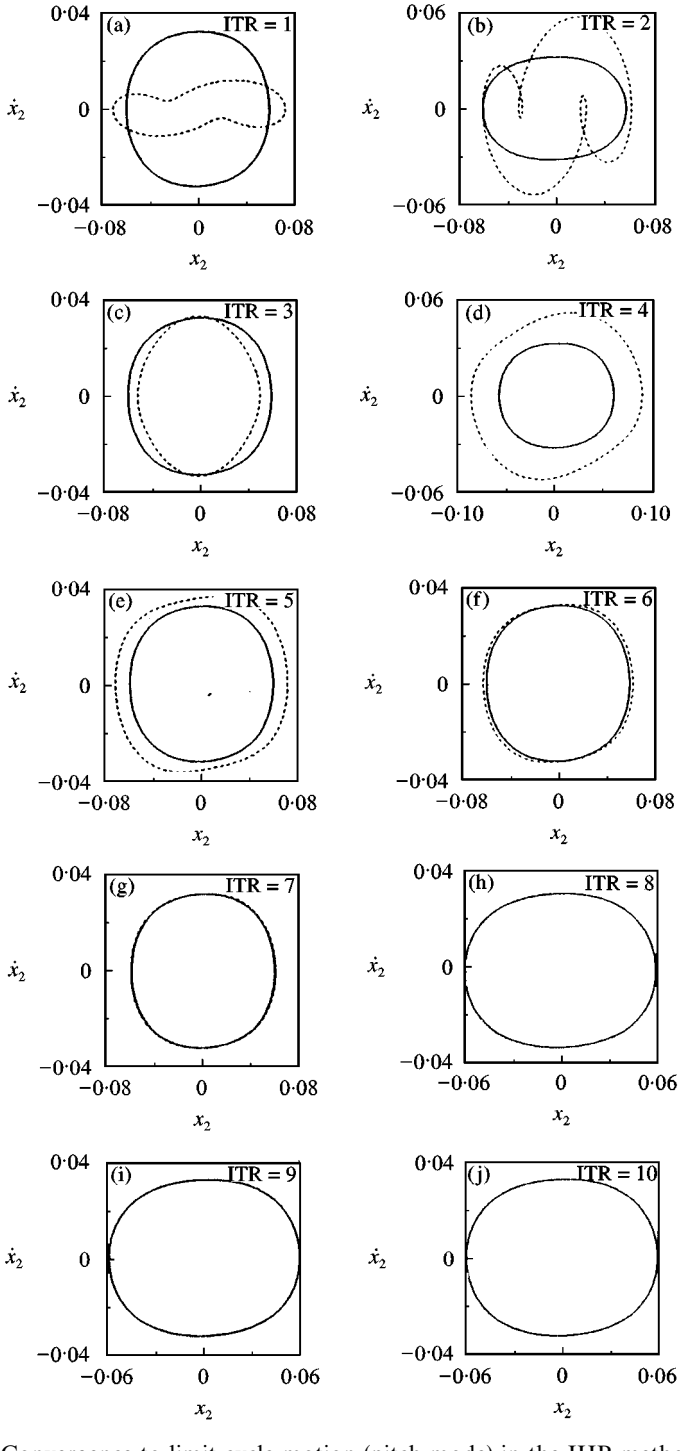

Figure 6. Convergence to limit cycle motion (pitch mode) in the IHB method $v = 3{\cdot}5$.

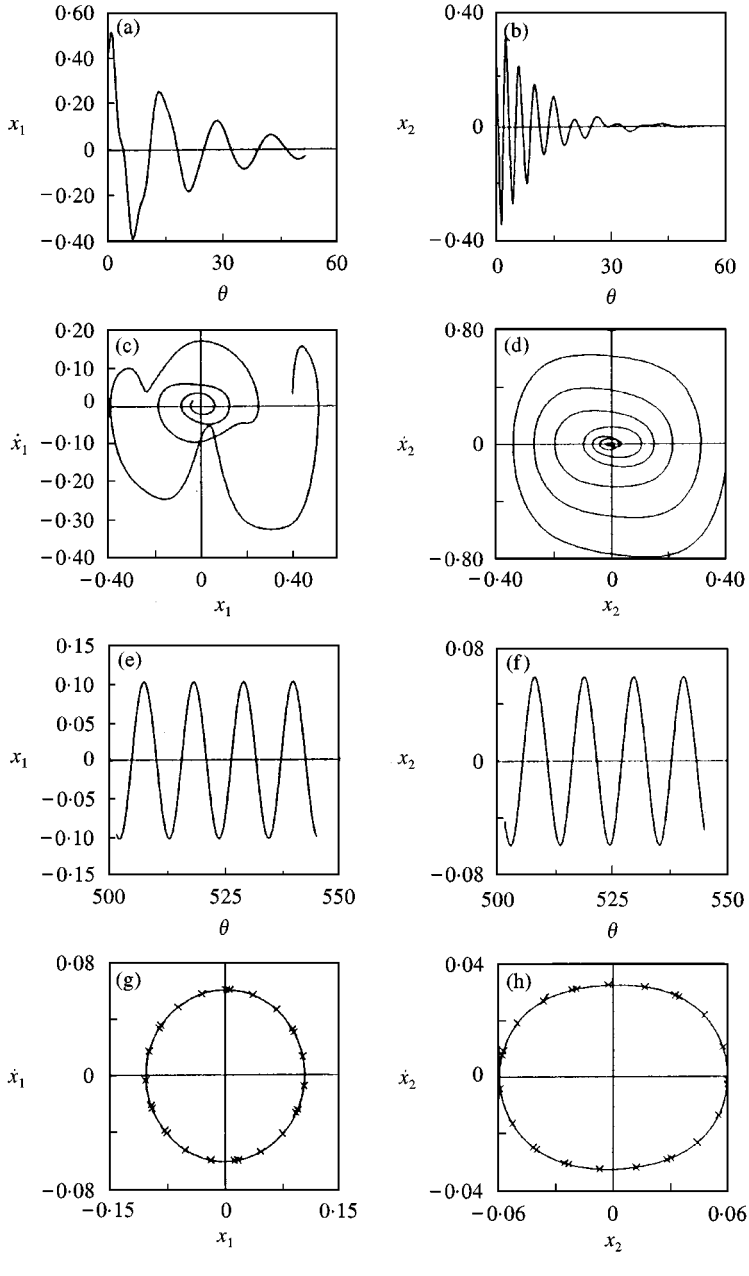

Figure 7. Motion settling to rest ($v = 0{\cdot}1$). (a) and (b) time histories (c) and (d) phase planes, Limit cycle motions ($v = 3{\cdot}5$), (e) and (f) time histories (g) and (h) phase planes.

It can be observed that at the end of the eighth iteration both the solutions merge together. This procedure is adopted for computing all the periodic and subharmonic motions and their frequencies in this section. The time histories and phase planes corresponding to the static state and limit cycle motion at $v = 0{\cdot}1$ and $3{\cdot}5$, respectively, are given in Figures 7(a)–(h). As v is increased further this periodic

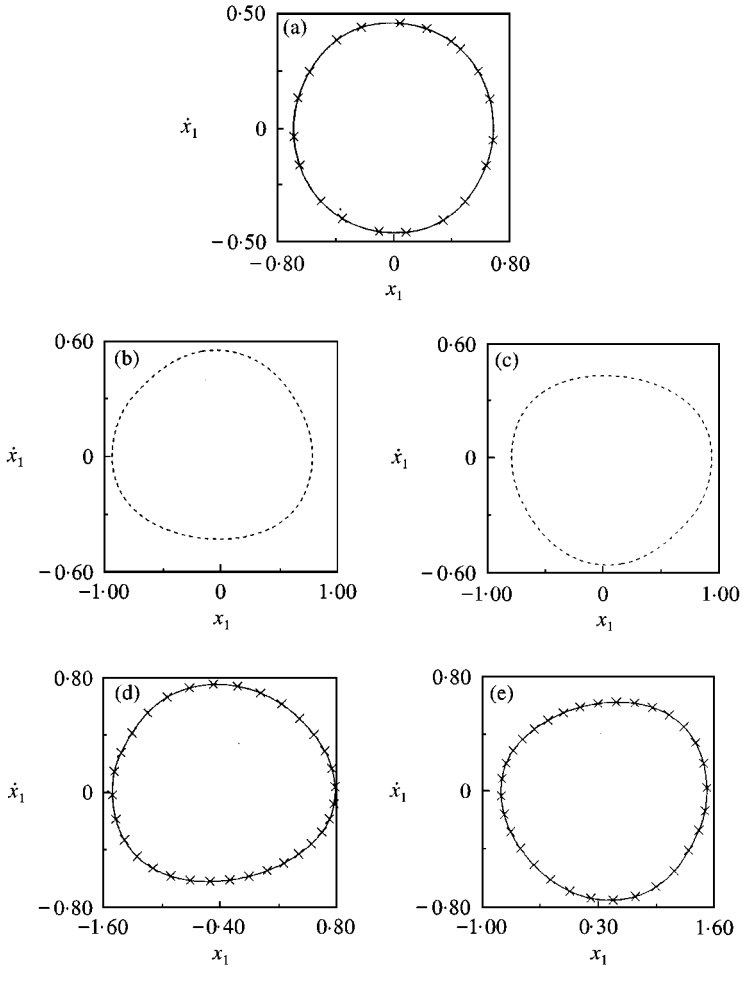

Figure 8. Phase plane diagrams, Plunge mode ($e = 20$, $d = 0{\cdot}07$, $v = 10$). (a) Symmetric period 1 motion, (b) and (c) unsymmetric unstable dual period 1 motions, (d) and (e) unsymmetric stable dual period 1 motions.

motion continues to exist till $v = 10{\cdot}80$ (point c in Figure 4) at which it becomes unstable indicated by the movement of the Floquet multiplier touching the unit circle and returning back indicating a symmetry breaking bifurcation. At point "c" two unstable and unsymmetric periodic motions emerge as v is decreased further indicated by the branches cd and cd′. These unsymmetric and unstable dual periodic motions become stable at d and d′ ($v = 8{\cdot}32$) at which one of Floquet multipliers enters the unit circle from the $+1$ direction indicating a saddle-node bifurcation. Thus in the region between cd and cd′ there exist one symmetric period 1, dual stable 1 and dual unstable period 1 responses. The phase planes of the five types of period 1 responses obtained by the IHB method are shown in Figures 8(a)–(e) and 9(a)–(e) for both the plunge and pitch modes respectively. The solid lines as usual indicate stable responses and the dashed lines indicate unstable responses. The stable solutions obtained by numerical integration are superposed

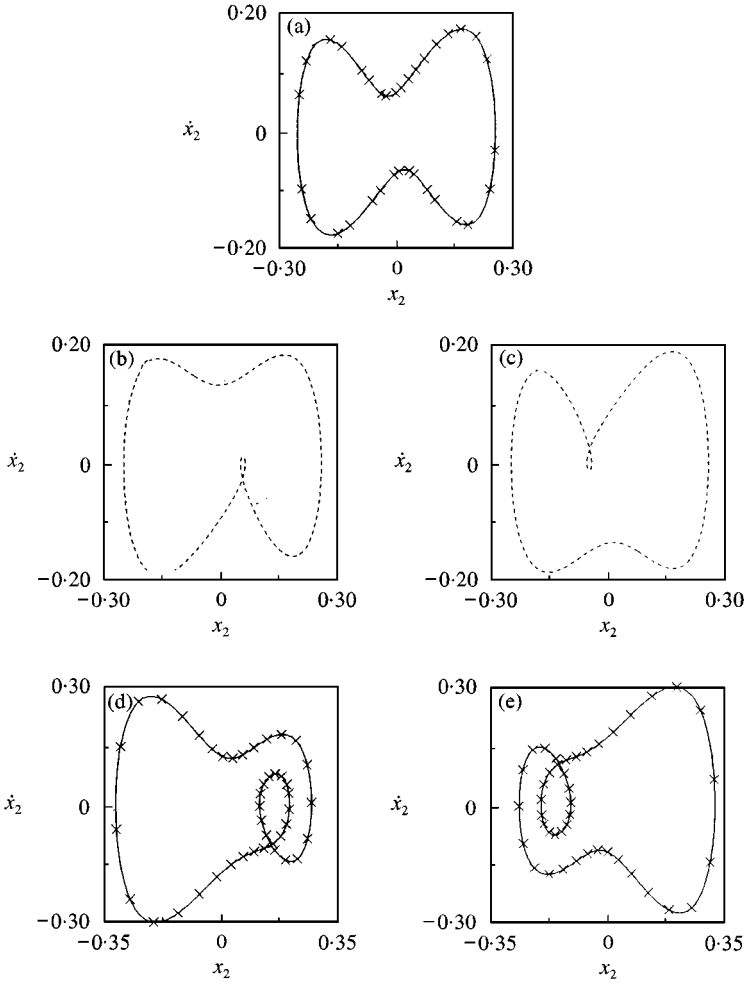

Figure 9. Phase plane diagrams, Pitch mode ($e = 20$, $d = 0{\cdot}07$, $v = 10$). (a) Symmetric period 1 motion, (b) and (c) unsymmetric unstable dual period motions, (d) and (e) unsymmetric stable dual period 1 motions.

by the "X" marks indicating once again the close fit between the IHB and numerically integrated solutions. In computing all these period 1 responses, eight harmonics were used in the finite Fourier series expansion.

Tracing these stable unsymmetric periodic solutions further by the path following method as v is increased, they remain stable till $v = 14{\cdot}76$ corresponding to the point e and e′. At this value the Floquet multiplier leaves the unit circle in -1 direction indicating a period doubling bifurcation. The dual period 1 motion gives rise to dual period 2 motion. Further increase in v results in a cascade of period-doubling bifurcations (points f and f′ at $v = 15{\cdot}07$) giving rise to dual period 4, period 8 motions, etc., ultimately leading to chaotic motion. The stable solution branches of the pitch mode are represented by solid lines and unstable branches by dashed lines in Figures 3(a), (b) and 4(a), (b). The corresponding phase planes of the period 2 and period 4 solutions obtained by the IHB method are shown in

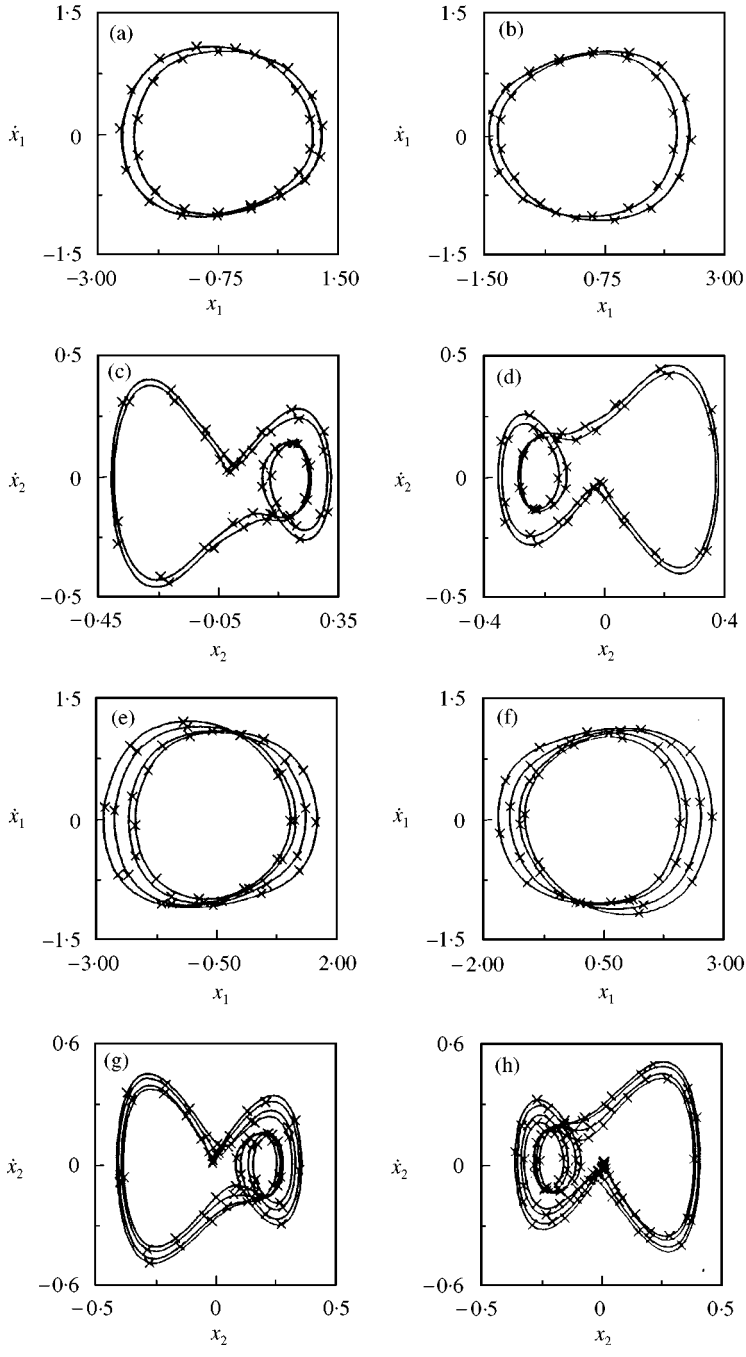

Figure 10. Phase plane diagrams, ($e = 20$, $d = 0{\cdot}07$). (a) and (b) dual period 2 motions ($v = 15{\cdot}0$, plunge mode), (c) and (d) dual period 2 motions ($v = 15{\cdot}0$, pitch mode) (e) and (f) dual period 4 motions ($v = 15{\cdot}4$, plunge mode) (g–h) dual period 4 motions ($v = 15{\cdot}4$, pitch mode).

Figures 10(a)–(h). The solutions obtained by numerical integration are superposed by the cross mark in the same figures indicating the close fit between the solutions obtained by the IHB method and by numerical integration. For obtaining the

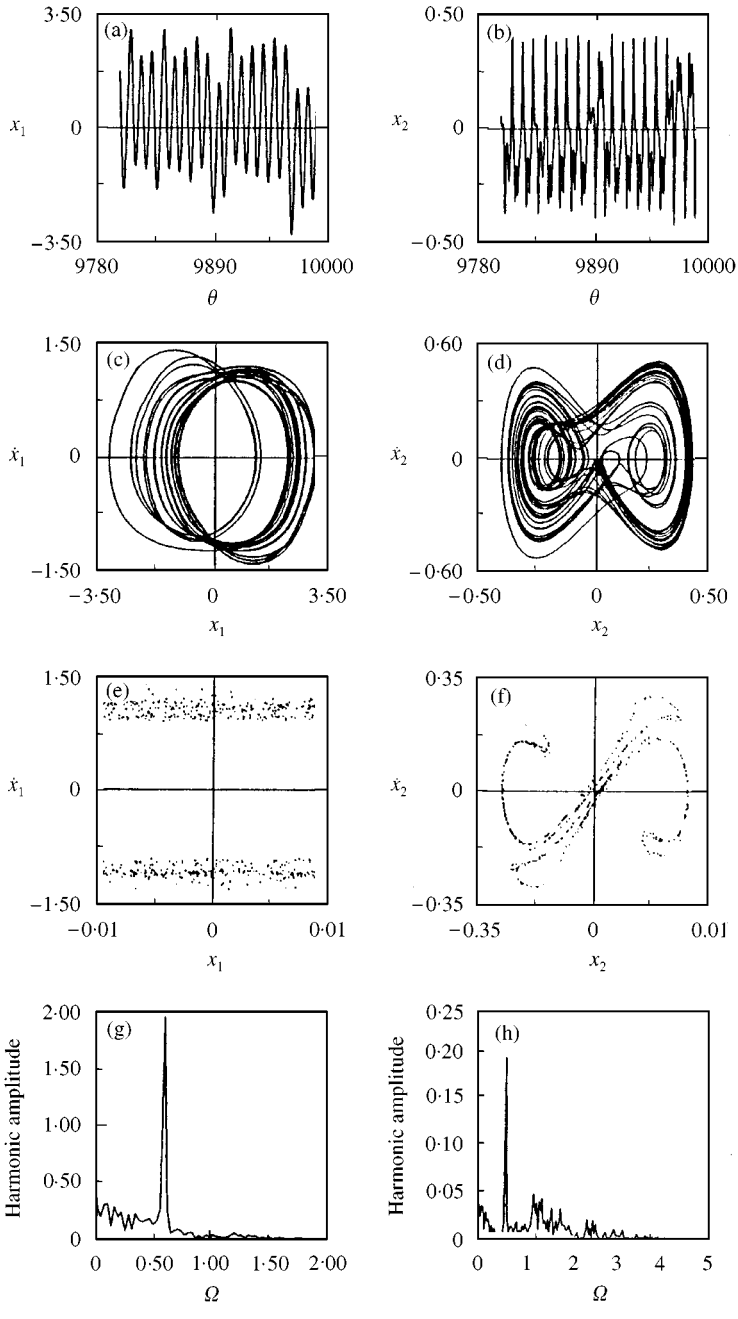

Figure 11. Chaotic motion ($e = 20$, $d = 0{\cdot}07$, $v = 15{\cdot}6$). (a) and (b) time histories, (c) and (d) phase planes, (e) and (f) Poincare' sections, (g) and (h) Fourier spectra.

period 2 solution by the IHB method 16 harmonics were used and for the period 4 solution 40 harmonics were used. The error criteria in the IHB method adopted for period 1 and period 2 solutions were $1{\cdot}0 \times 10^{-05}$ and for the period 4 solution was $1{\cdot}0 \times 0^{-03}$.

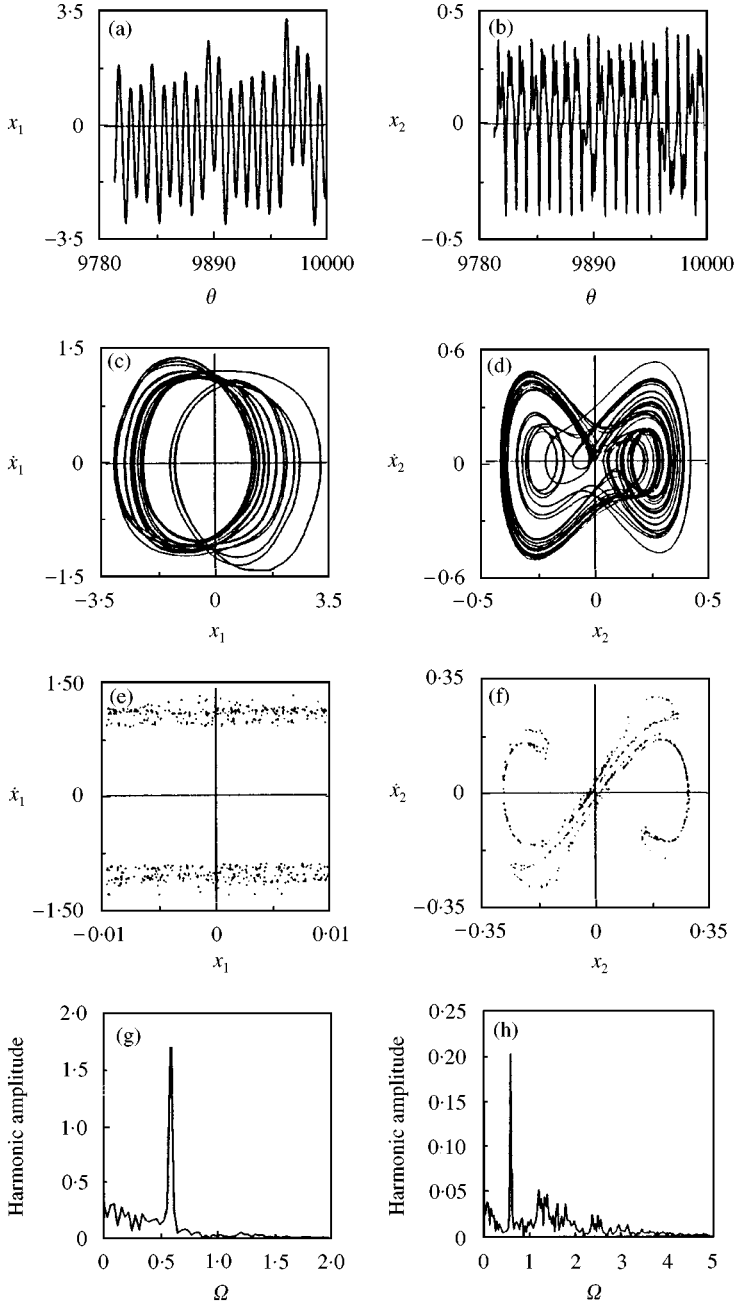

Figure 12. Dual chaotic motion ($e = 20$, $d = 0{\cdot}07$, $v = 15{\cdot}6$, $v = 15{\cdot}6$). (a) and (b) time histories, (c) and (d) phase planes, (e) and (f) Poincare' sections, (g) and (h) Fourier spectra.

The time histories, phase planes, Poincare' sections and Fourier spectra of the dual chaotic response computed by numerical integration are shown in Figures 11(a)–(h) and 12(a)–(h). As the system is autonomous, strictly the Poincare' section should be a horizontal line for one of the modes. But in the numerical computation it is difficult to get this section exactly for a particular mode, and hence the section

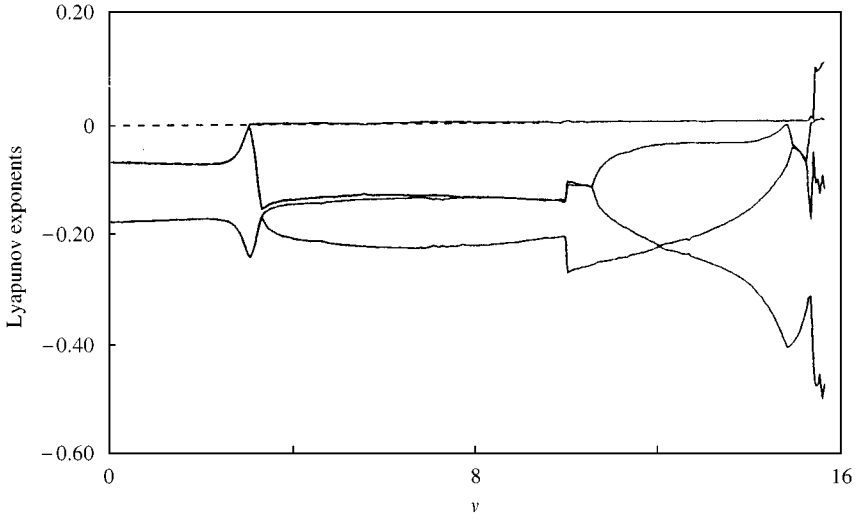

Figure 13. Lyapunov exponents.

is taken over a small range of plunge-mode displacement between $-0{\cdot}01$ and $0{\cdot}01$. It is seen that the Poincare' section shows a typical strange attractor behavior. The type of motions exhibited also compare very well with that of Zhao and Yang [4] obtained by numerical integration.

The Lyapunov exponents are computed using the algorithm given by Wolf *et al.* [17]. They are shown in Figure 13. It can be observed that the largest Lyapunov exponent becomes positive in the region of chaos and the typical value of the positive Lyapunov exponent at $v = 15{\cdot}60$ is $0{\cdot}1070$.

7. CONCLUSION

In this paper, the periodic motions of a self-excited two-dimensional airfoil in pitch and bounce with cubic pitching stiffness are obtained by the IHB method. The system exhibits complex dynamical behavior such as limit cycle motions, multiple responses, subharmonic responses and chaotic motion. A path following procedure traces the bifurcation behavior and shows an initial Hopf bifurcation of zero type, symmetry breaking bifurcation and period-doubling bifurcations leading to chaotic motion. The periodic and subharmonic motions computed by the IHB method agree very well with those obtained by numerical integration. The unknown frequency of the limit cycle oscillation of the autonomous system is also obtained by the IHB method. This demonstrates the ability of the IHB method in accurately obtaining the periodic motions of the two-degrees-of-freedom non-linear autonomous system and the efficacy of the path following procedure in combination with the IHB method in obtaining the bifurcation behavior.

REFERENCES

1. E. H. Dowell 1992 *Journal of Sound and Vibration* **85**, 333–344. Flutter of a buckled plate as an example of chaotic motion of a deterministic autonomous system.

2. E. H. Dowell and M. Ilgamov 1988 *Studies in Nonlinear Aeroelasticity*. New York: Springer.
3. Z. C. Yang and L. C. Zhao 1988 *Journal of Sound and Vibration* **123**, 1–13. Analysis of limit cycle flutter of an airfoil in incompressible flow.
4. L. C. Zhao and Z. C. Yang 1990 *Journal of Sound and Vibration* **138**, 245–254. Chaotic motions of an airfoil with nonlinear stiffness in incompressible flow.
5. D. M. Tang and E. H. Dowell 1992 *Journal of Aircraft* **29**, 953–960. Flutter and stall response of a helicopter blade with structural nonlinearity.
6. S. J. Price and H. Alighanbari 1995 *Journal of Fluids and Structures* **9**, 175–193. The aeroelastic response of a two dimensional airfoil with bilinear and cubic structural nonlinearities.
7. S.-H. Kim and I. Lee 1996 *Journal of Sound and Vibration* **193**, 823–846. Aeroelastic analysis of a flexible air-foil with a freeplay nonlinearity.
8. M. D. Conner, D. M. Tang, E. H. Dowell and L. N. Virgin 1997 *Journal of Fluids and Structures* **11**, 89–109. Nonlinear behavior of a typical airfoil section with control surface freeplay: a numerical and experimental study.
9. Y. K. Cheung and S. L. Lau 1982 *Earthquake engineering and structural dynamics* **10**, 239–253. Incremental time–space finite strip method for nonlinear structural vibrations.
10. S. L. Lau, Y. K. Cheung and S. Y. Wu 1982 *Journal of Applied Mechanics* **49**, 849–853. A variable parameter incrementation method of dynamic instability of linear and nonlinear systems.
11. A. Y. T. Leung and T. C. Fung 1989 *Journal of Sound and Vibration* **131**, 445–455. Construction of chaotic regions.
12. S. H. Chen, Y. K. Cheung and S. L. Lau 1991 *International Journal of Nonlinear Mechanics* **26**, 125–133. On perturbation procedure for limit cycle analysis.
13. S. L. Lau and S. W. Yuen 1993 *Journal of Sound and Vibration* **167**, 303–316. Solution diagram of nonlinear dynamic systems by the IHB method.
14. A. Y. T. Leung and S. K. Chui 1995 *Journal of Sound and Vibration* **181**, 619–633. Nonlinear vibration of coupled duffing oscillators by an improved incremental harmonic balance method.
15. Y. C. Fung 1968 *An Introduction to the Theory of Aeroelasticity. Inc, New York*: *Dover Publication.*
16. P. Friedmann, C. E. Hammond and T. H. Woo 1977 *International Journal of Numerical Methods in Engineering* **11**, 1117–1136. Efficient numerical treatment of periodic systems with application to stability problems.
17. J. B. S. Wolf, H. L. Swinney and J. A. Vastano 1985 *Physica* **16D**, 285–317. Determining Lyapunov exponents from a time series.

APPENDIX A. FOURIER SERIES EXPANSION FOR PRODUCT OF DISPLACEMENT VECTORS AND TERMS APPEARING IN EQUATIONS (19) AND (20)

Consider an assumed solution given by the finite Fourier series of the form

$$x(\tau) = a_0 + \sum_{i=0}^{N} (a_i \cos i\tau + b_i \sin i\tau).$$

The vector double product is given by

$$x^2(\tau) = A_0 + \sum_{k=1}^{2N} (A_k^c \cos k\tau + A_k^s \sin k\tau).$$

In order to derive the expressions for A_0, A_k^c, A_k^s, considering only two harmonic coefficients in the series, we have

$$x(\tau) = a_0 + a_1 \cos\tau + a_2 \cos 2\tau + b_1 \sin\tau + b_2 \sin 2\tau,$$

$$\begin{aligned} x^2(\tau) = {} & a_0^2 + a_0 a_1 \cos\tau + a_0 a_2 \cos 2\tau + a_0 b_1 \sin\tau + a_0 b_2 \sin 2\tau \\ & + a_0 a_1 \cos\tau + a_1^2 \cos^2\tau + a_1 a_2 \cos\tau \cos 2\tau + a_1 b_1 \cos\tau \sin\tau \\ & + a_1 b_2 \cos\tau \sin 2\tau + a_0 a_2 \cos 2\tau + a_1 a_2 \cos\tau \cos 2\tau + a_2^2 \cos^2 2\tau \\ & + a_2 b_1 \cos 2\tau \sin\tau + a_2 b_2 \cos 2\tau \sin 2\tau \\ & a_0 b_1 \sin\tau + a_1 b_1 \cos\tau \sin\tau + a_2 b_1 \cos 2\tau \sin\tau + b_1^2 \sin^2\tau + b_1 b_2 \sin\tau \sin 2\tau. \end{aligned}$$

By applying the trigonometric sum and product rule and collecting the terms corresponding to $\cos 0\tau$, $\cos\tau$, $\cos 2\tau$, $\cos 3\tau$, $\cos 4\tau$ and $\sin 0\tau$, $\sin\tau$, $\sin 2\tau$, $\sin 3\tau$, $\sin 4\tau$, we get

$$\begin{aligned} x^2(\tau) = {} & (a_0^2 + 1/2(a_1^2 + b_1^2 + a_2^2 + b_2^2)) \cos 0\tau \\ & + (2a_0 a_1 + a_1 a_2 + b_1 b_2) \cos\tau + (2a_0 a_2 + (\tfrac{1}{2}) a_1^2 - (\tfrac{1}{2}) b_1^2) \\ & + (a_1 a_2 - b_1 b_2) \cos 3\tau + ((\tfrac{1}{2}) a_2^2 - (\tfrac{1}{2}) b_2^2) \cos 4\tau \\ & + (2a_0 b_1 + a_1 b_2 - a_2 b_1) \sin\tau + (2a_0 b_2 + a_1 b_1) \sin 2\tau \\ & + (a_1 b_2 + a_2 b_1) \sin 3\tau + a_2 b_2 \sin 4\tau. \end{aligned}$$

In this way, the coefficients A_0, A_k^c, A_k^s can be generalized for the series having N number of harmonics as

$$A_0 = a_0^2 + \frac{1}{2} \sum_{i=1}^{N} (a_i^2 + b_i^2),$$

$$A_k^c = A_{k1}^c + A_{k2}^c + A_{k3},$$

$$A_{k1}^c = \begin{cases} 2a_0 a_k & \text{if } k \leqslant N, \\ 0 & \text{otherwise,} \end{cases}$$

$$A_{k2}^c = \begin{cases} \dfrac{1}{2} \displaystyle\sum_{i=1}^{N} (a_{i+k} a_i + b_{i+k} b_i) & \text{if } (i+k) \leqslant N, \\ 0 & \text{otherwise,} \end{cases}$$

$$A^c_{k3} = \begin{cases} \frac{1}{2}\sum_{i=1}^{N} (a_{|i-k|}\, a_i + \operatorname{sgn}(i-k)\, b_{|i-k|}\, b_i & \text{if } |i-k| \leqslant N \text{ and } |i-k| \geqslant 1, \\ 0 & \text{otherwise,} \end{cases}$$

$$A^s_k = A^s_{k1} + A^s_{k2} + A^s_{k3},$$

$$A^s_{k1} = \begin{cases} 2a_0 b_k & \text{if } k \leqslant N, \\ 0 & \text{otherwise,} \end{cases}$$

$$A^s_{k2} = \begin{cases} \frac{1}{2}\sum_{i=1}^{N} (b_{i+k}\, a_i - a_{i+k}\, b_i) & \text{if } (i+k) \leqslant N, \\ 0 & \text{otherwise,} \end{cases}$$

$$A^s_{k3} =$$

$$\begin{cases} \frac{1}{2}\sum_{i=1}^{N} (\operatorname{sgn}(k-i)\, b_{|i-k|}\, a_i + \operatorname{sgn}^2(k-i) a_{|i-k|}\, b_i & \text{if } |i-k| \leqslant N \text{ and } |i-k| \geqslant 1, \\ 0 & \text{otherwise.} \end{cases}$$

The vector triple product is given by

$$x^3(\tau) = B_0 + \sum_{k=1}^{3N} (B^c_k \cos k\tau + B^s_k \sin k\tau),$$

$$B_0 = A_0\, a_0 + \tfrac{1}{2}\sum_{i=1}^{N} (A^c_i\, a_i + A^s_i\, b_i),$$

$$B^c_k = B^c_{k1} + B^c_{k2} + B^c_{k3},$$

$$B^c_{k1} = \begin{cases} A_0\, a_k & \text{if } k \leqslant N, \\ 0 & \text{otherwise,} \end{cases}$$

$$B^c_{k2} = \begin{cases} A^c_k\, a_0 & \text{if } k \leqslant 2N, \\ 0 & \text{otherwise,} \end{cases}$$

$$B^c_{k3} = \begin{cases} \frac{1}{2}\sum_{i=1}^{N} (A^c_{i+k}\, a_i + A^s_{i+k}\, b_i) & \text{if } (i+k) \leqslant 2N \\ 0 & \text{otherwise,} \end{cases}$$

$$B_{k4}^c = \begin{cases} \frac{1}{2}\sum_{i=1}^{N} (A_{|i-k|}^c a_i + \operatorname{sgn}(i-k) A_{|i-k|}^s b_i & \text{if } |i-k| \leqslant 2N \text{ and } |i-k| \geqslant 1, \\ 0 & \text{otherwise,} \end{cases}$$

$$B_k^s = B_{k1}^s + B_{k2}^s + B_{k3}^s,$$

$$B_{k1}^s = \begin{cases} A_0 b_k & \text{if } k \leqslant N, \\ 0 & \text{otherwise,} \end{cases}$$

$$B_{k2}^s = \begin{cases} A_k^s a_0 & \text{if } k \leqslant 2N, \\ 0 & \text{otherwise,} \end{cases}$$

$$B_{k3}^c = \begin{cases} \frac{1}{2}\sum_{i=1}^{N} (A_{i+k}^s a_i - A_{i+k}^c b_i) & \text{if } (i+k) \leqslant 2N, \\ 0 & \text{otherwise,} \end{cases}$$

$$B_{k4}^c = \begin{cases} \frac{1}{2}\sum_{i=1}^{N} (A_{|i-k|}^c b_i + \operatorname{sgn}(k-i) A_{|k-i|}^s a_i & \text{if } (i-k) \leqslant 2N \text{ and } |i-k| \geqslant 1, \\ 0 & \text{otherwise.} \end{cases}$$